Indian Journal of Engineering & Materials Sciences
Vol. 31, August 2024, pp. 474-486
DOI: 10.56042/ijems,v31i4.2596

Review Article

Performance evaluation of newly developed slotted modulator of co-axial magnetic gears

Yang Chaojun[a,b], Amberbir Wondimu[a], Gu Lixiang[a] & Qi Yutang[a]

[a]Jiangsu University, School of Mechanical Engineering, Zhenjiang, 212013, China

[b]State Key Laboratory of Mechanical Transmission for Advanced Equipment, Chongqing University, Chongqing 400044, China

Received: 12 June 2023; Accepted: 23 May 2024

A modulator and a connecting bridge have made up the magnetic modulator ring in co-axial magnetic gears (CMG). This critical review has examined the combined influence of modulator bridge configuration and varying magnetization on the functionality of a recently created slotted modulator in the CMG model. The magnetic flux density and static torque of the CMG with various structural configurations of the slotted modulating rings have been evaluated using the two-dimensional nonlinear finite element method. Based on the bird's-eye view of the review, the inner modulator bridge with Halbach array magnetization has been found to be the best combination to perform well among the other two combinations. The slotted modulator bridge positions in the center and outer locations have been shown to reduce the magnetic flux density distribution by 4.5% and 9.9%, respectively, when compared to the inner position. Furthermore, the maximum static torque obtained at the inner bridge position and Halbach magnetization has been 169 Nm, which shows a 1.071% improvement. Therefore, this critical analysis recommends using a thinner inner modulator bridge combined with a Halbach array configuration to boost CMG performance.

Keywords: Bridge configurations, Slotted modulator, Magnetization, Magnetic flux density, Static torque

1 Introduction

Mechanical gears can produce large torque densities; the industry has employed them extensively in power transmission applications. However, they are vulnerable to a number of issues, including noise, friction, the need for lubrication, fatigue, which results in regular maintenance, and poor reliability[1]. The reliable performance of electromechanical systems has always been a major concern with the advancement of industrial technology[2] and the creation of novel energy technologies[3]. The transmission system has always had a mechanical gear as a key component[4]. Therefore, higher-quality gear needs to be designed to replace it. Magnetic gears (MG) is a non-contact magnetic force-driven electromagnetic devices that have the advantages of being low-noise[5], low-vibration[6], free of maintenance, and overload-protective by nature. Currently, MG are employed in a variety of low-speed and high-torque applications[7], particularly when permanent magnet motors are involved, such as electric vehicles[8, 9], wind turbines[10-15], maritime electric propulsion[16, 17], aerospace[18], and traction[19].

The most typical CMG setup comprises a pair of concentric iron yokes, the permanent magnets attached to them, and a flux-modulator ring positioned in the middle[20-23]. It is imperative for the CMG to function properly that the total number of iron pole pieces utilized in the modulator ring equals the entire number of permanent magnet pole pairs in both the inner and outer rotors[24]. Additionally, the quotient of the total number of pole pieces in the outer rotor and the number of pole pieces in the inner rotor is identical to the hypothetical equivalent gear ratio of CMG in the context of a stationary modulator ring. With the objective of boosting torque density, the CMG has been extensively addressed in the literature[25-31].

The design incorporates stationary pole components distributed between the inner and outer rotors. This allows the design to withstand the shear stress exerted on the surfaces where the inner and outer rotors are in contact[32]. To address the drawbacks of conventional designs, this new approach utilizes bridges to connect the stationary pole parts, or modulators[33]. The air-gap flux density distribution in the CMG bridges has a significant influence on the maximum torque the system can transmit. However, these bridges tend to prevent modulation of the air gap flux density due to the considerable flux leakage they produce. This flux leakage lowers torque production and transfer on both the inner and outer

*Corresponding author (E-mail: ambirewondimu@gmail.com)

rotors, ultimately leading to increased iron losses in the modulator parts[34-36]. In addition to the bridge design, various other factors can influence the performance of CMG, such as: gear ratios[3], the thickness of the modulator[36], modulator shape[36], modulator carriage bridge configuration[36], air gap thickness[37], magnetization[38], magnetic materials[39] and others.

It is important to discuss the progress of computing tools while evaluating the performance of magnetic gears. Hence, the performance of MG can be analyzed through a variety of techniques, including the analytical method[40, 41], the equivalent magnetic circuit approach[42], finite element analysis[43-45], and the AI-based field approximation method[43-47]. The existing computation techniques do have certain drawbacks. The FE method is a reliable simulation tool, but meshing, forming the global matrix, and matrix inversion are computationally intensive activities. The analytical method uses little computational power, and generalizability is constrained. AI-based field estimation provides a different strategy for easily evaluating the performance of MG. With the ongoing advancement of data-driven methodologies, they have steadily been employed for difficult data fitting[46-51]. Magnetic field estimation has been the subject of both supervised and unsupervised learning approaches[51-54].

This critical review presents a performance evaluation of the new slotted modulator-based CMG design. Based on findings from previous studies, this analysis provides insights on how to increase the performance and address the challenges of this new CMG design. The second section offers clear insights on modulation techniques for CMG as well as an evaluation of the impacts of various modulator bridge positions and thicknesses on its performance. Using COMSOL Multiphysics, Section 3 presents a 2D nonlinear finite element-based electromagnetic performance evaluation of the slotted modulator bridges and magnetization for the new CMG model. Lastly, the review suggests the best combination of modulator bridge position and magnetization to improve the performance and applicability of CMG with a slotted modulator ring design.

2 Materials and Methods

2.1 Principles of modulation

One of the most important factors to take into account while choosing magnetic gears, especially for industrial applications, is their structural topologies. As a result, there are two types of MG topologies: non-modulated and modulated.

2.1.1 Non modulated magnetic gears

These topologies, as depicted in Fig. 1, referred to as conventional magnetic gears or non-contact MG, allow permanent magnets (PMs) to be arranged in a variety of ways that interact magnetically to convey torque. Permanent magnets are less likely to be used in the majority of industries owing to their poor performance[55-61]. The radial and tangential flux densities produced by any permanent magnetic rotor at radial distance r can be stated as, in the absence of a modulating component, given as follows:

$$B^0{}_r(r,\theta) = \sum_{m=1,3,5....} b_{rm}(r)cos[mp(\theta - \omega_r t) + mp\theta_0] \quad (1)$$

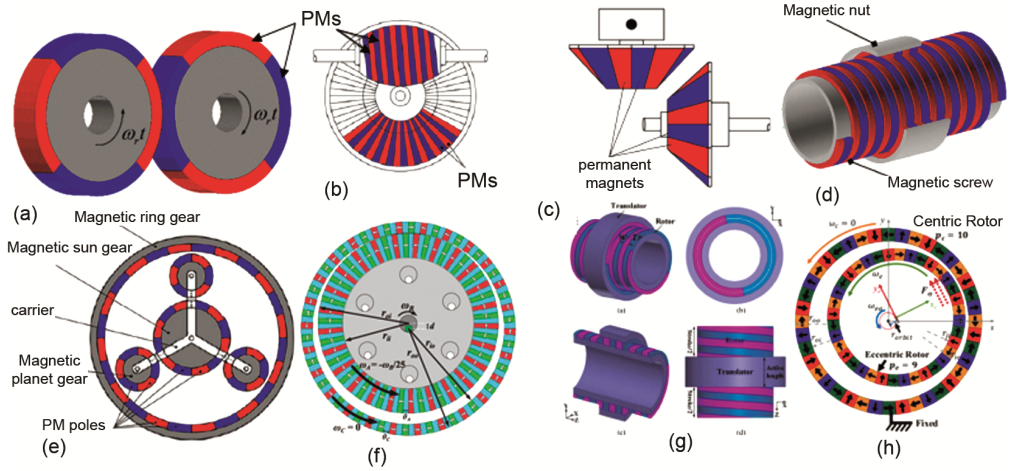

Fig. 1 — Magnetic gears without modulators (a) Spur MG[55], (b) Worm MG[56], (c) Perpendicular[57], (d) Magnetic screw, (e) Planetary[58], (f) Cycloid[59], (g) Trans-rotary[60], and (h) Harmonic type of MGs[61]

Table 1 — Summery on conventional (non-modulated) MGs and limitations based on Fig. 1

Type	Limitations	Applications
(a)	Less torque density as a result of improper PM usage	Less in Industrial Applications
(b)		
(c)		
(d)	There have been very few research on this MGs topology	
(e)	Fairly high torque density than shown on (a-d)	Useful in high gear ratio industrail applications
(f)	Have significant gear reduction ability	
(g)	When compared to the preceding topologies (a-f), have higher efficiency and torque density.	Particularly useful in situations where linear motion must be converted to rotating motion.
(h)	Torque ripple-free and advantageous in situations requiring a high gear ratio	Manufacturing is difficult, making it unsuitable for many applications

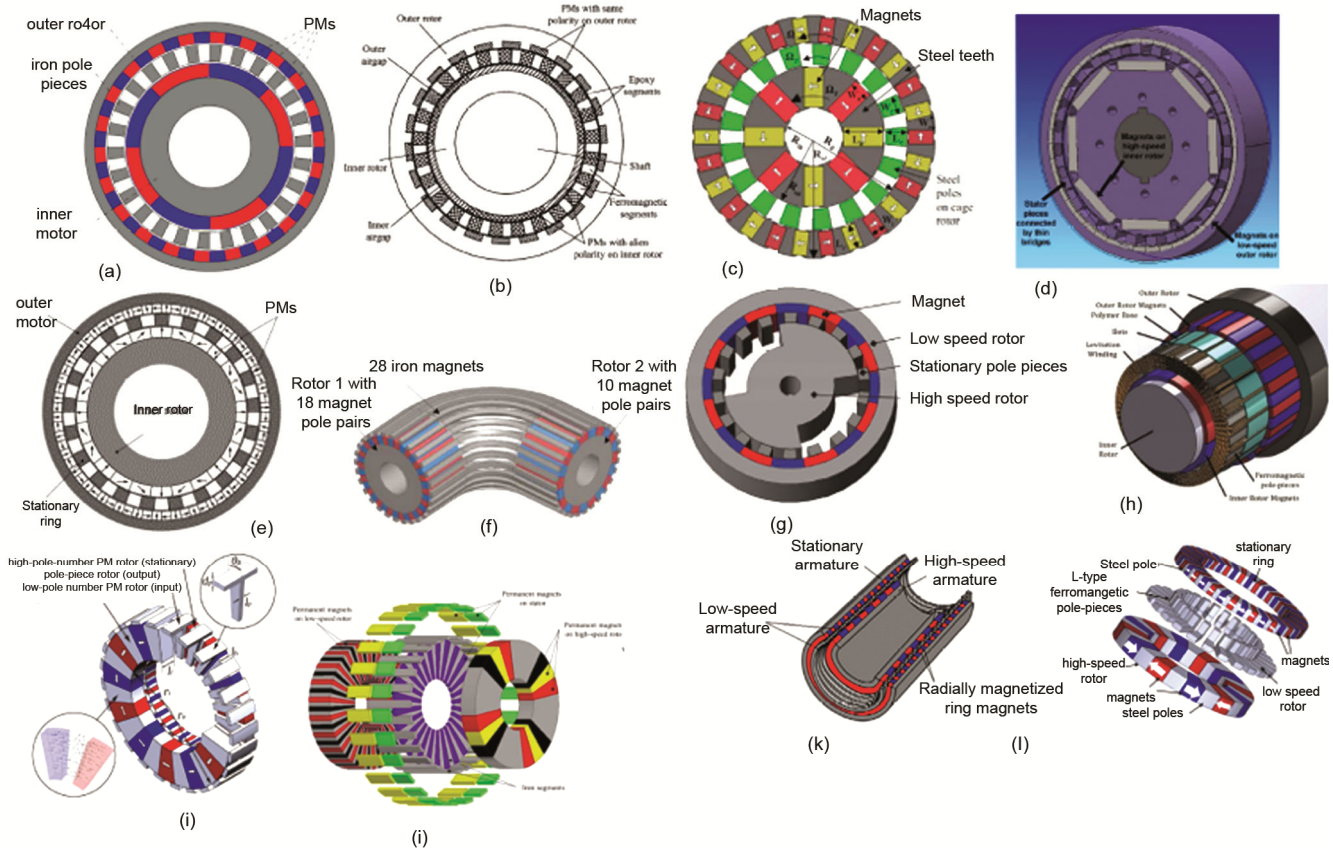

Fig. 2 — Magnetic gears with mudulators (a). Spur MG[12], (b). Homopolar IPM MG[13], (c). Spoke MG[14], (d).IPM MG[15], (e). Halbach MG[16], (f). Intersecting-axes MG[17]. (g). Reluctance MG[18]. (h). Bearingless MG[19], (i). T-shaped axial MG[20], (j). Hybrid-flux MG[21], (k). Linear MG[22], (l). L-shaped axial MG[23].

$$B^0{}_\theta(r,\theta) = \sum_{m=1,3,5....} b_{\theta m}(r)cos[mp(\theta - \omega_\theta t) + mp\theta_1] \quad (2)$$

where ω_r is the angular velocity of the rotor, p is the number of pole pairs in the PM, and m is the harmonic order; the magnetic flux density distribution's initial radial and tangential angles are θ and θ_1, respectively; the Fourier coefficients are b_{qm} and b_{rm}.

2.1.2 Modulated topologies of magnetic gears

This topologies are the most promising type, owing to its high efficiency and torque density as compared to the corresponding non modulated topologies of MG[62-68]. Due to the presence of the modulator, as shown in Fig. 2, the magnetic field that's created by the PMs of the inner and outer rotor can be altered, resulting in the generation of numerous spatial harmonics in both air gaps adjacent to the modulator[63].

Modulator's tangential and radial modulating functions can be written as follows:

$$\lambda_r(r,\theta) = \lambda_{ro}(r) + \sum_{j=1,2,3....} \lambda_{rj}(r)cos(jn_s(\theta - \omega_r t)) \quad (3)$$

$$\lambda_\theta(r,\theta) = \lambda_{\theta o}(r) + \sum_{j=1,2,3....} \lambda_{\theta j}(r)sin(jn_s(\theta - \omega_r t)) \quad (4)$$

Where n_s is the number of modulators, $\lambda_{r0}, \lambda_{\theta 0}, \lambda_{rj}$, and $\lambda_{\theta j}$ are Fourier coefficients, and j is the harmonic order. Therefore, the modulator's modulation of the air gap's radial and tangential magnetic flux concentrations is as follows:

$$B_r(r,\theta) = B^0{}_r(r,\theta) \cdot \lambda_r(r,\theta) \quad (5)$$

$$B_\theta(r,\theta) = B^0{}_\theta(r,\theta) \cdot \lambda_\theta(r,\theta) \quad (6)$$

Both the inner and outer air-gap magnetic fields are primarily influenced by the modulator, resulting in an efficient coupling between the two fields to provide the desired torque. From Eqs. (5) and (6), it can be deduced that the total number of pole pairs and spinning of space harmonics induced by any PM rotor speed meet the condition as follows:

$$P_{m,k} = |mp + kn_s| \quad (7)$$

$$\Omega_{m,k} = \frac{mp}{mp+kn_s}\Omega_r + \frac{kn_s}{mp+kn_s}\Omega_s \quad (8)$$

Where –p- is the number of the pole pair of both inner or outer rotor PMs and m = 1, 3, and 5..., k = 0, 1... The space harmonics' angular velocities are m, and $\Omega_{m,k}$; both inner and outer rotor angular velocity are Ω_r; and the modulator's angular velocity is Ω_s.

The rotor PM's number of pole pairs needs to conform to the following interactions:

$$P_{in}+P_{out} = n_s \quad (9)$$

Whereas P_{in} and P_{out} are identified as the PMs pole pairs for the inner and outer rotors accordingly, the MGs gear ratio can be written as:

$$G_r = \frac{P_{out}}{P_{in}} \quad (10)$$

Figure 3 depicts various topologies and arrangements of the magnetic modulation ring that are commonly used by researchers. There are three modulators of unique shapes, depicted in Fig. 3(a) as a square modulator, Fig. 3(b) as an arc modulator, and Fig. 3(c) as a circular modulator.

Each modulator shape is illustrated by five positions of bridge modulators: the innermost Fig. 4 (a), the inner Fig. 4 (b), the center Fig. 4 (c), the outer Fig. 4 (d) and the outermost Fig. 4 (e).

The following performance comparison is made based on the obtained data from[63-66]. First, keeping the thickness of the modulator bridge constant, the impact of the modulator bridge's location is evaluated as shown in Figs 5 and 6, with the best position of the modulator bridge suggested; second, the impact of varying the modulator bridge's thickness has been evaluated. Lastly, based on the evaluation, this study suggests the best position of the modulator bridge for CMG in various applications.

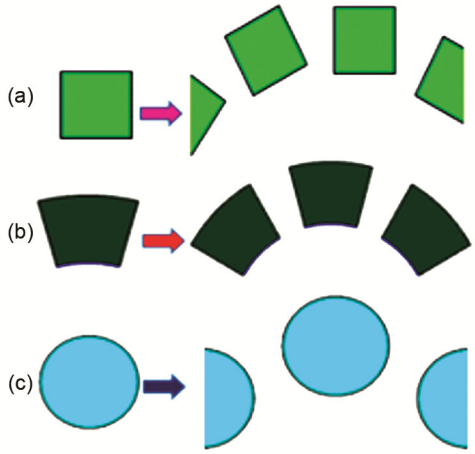

Fig. 3 — Three commonly used shapes of modulator, (a). Square, (b). Arc, (c). Circular type topologies[65, 66].

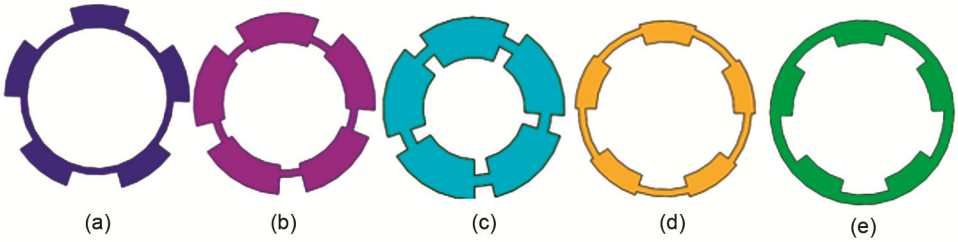

Fig.4 — Various modulator and its bridge configurations, (a). Inner most, (b).Inner, (c). Center, (d). Outer, e). Outer most[65, 66].

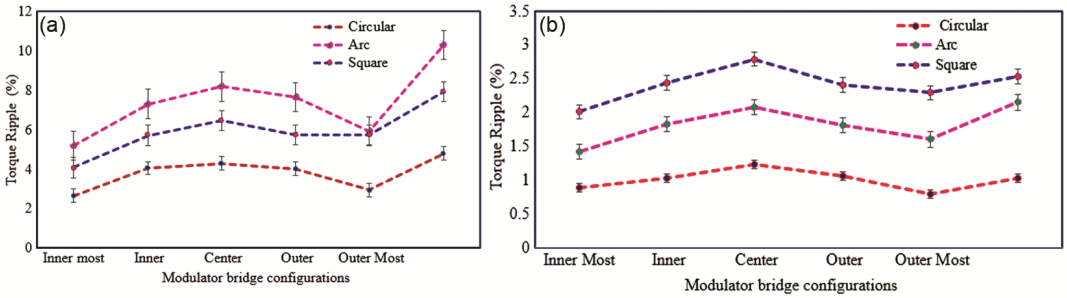

Fig. 5 — Torque ripple vs. modulator bridge configurations, a) Inner rotor, and b) Outer rotor, data taken and reproduced [64-66].

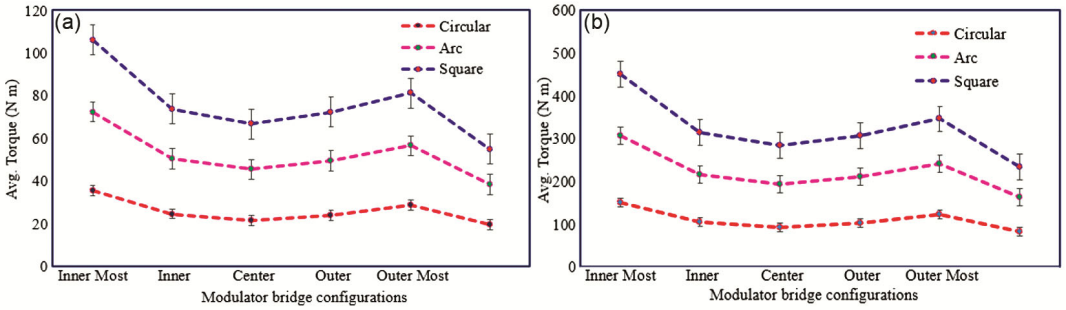

Fig. 6 — Average torque vs. modulator bridge configuration (a). Inner rotor, (b). Outer rotor, data taken and reproduced[64-66].

2.1.3 Performance comparison of three modulator shapes

To make the comparison precise and consistent, the modulator thickness is assumed to be the same in all configurations and is set at $3^{*}\ 10^{-3}$m. The inner modulator bridge provides the least torque ripple for both the inner Fig. 5(a) and outer Fig. 5(b) rotors, in contrast to the outermost bridge, which creates the greatest torque ripple for both the inner and outer rotors. The use of a circular modulator decreases inner torque ripple in all modulator bridge positions, but the execution of a square modulator is worse in all joining bridge arrangements at the outer rotor and causes serious torque ripple. The average torque versus modulator carriage bridge configuration, inner most (IM) is best position get average torque for both high and low speed rotors in contrast to the outermost (OM) configuration, see Fig. 6 (a) and (b). Square modulator shape have better performance than the other two modulator topologies.

2.1.4 Impact of bridge thickness on the CMG performance

The torque ripple, for the outer, center bridge modulator configurations on CMG consistently increases up to 38.46%, and 11.12%, respectively, and drops by 14.28% for the inner bridge position with a bridge thickness is $1^{*}10^{-3}$m as shown in Fig. 7 (a). A similar trend of the results is shown in Fig.7 (b) for the outer rotor, the outer and center-bridge modulators configurations consistently increase up to 66.67%, and 54.56%, respectively, and drop by 120.21% for the inner bridge position as a function of the three bridge positions and thickness.

For the certain inner rotor rotating speed, Fig.7(c) examines the iron losses according to the placement and bridges thickness (mm). The iron loss quickly increased to 125.93% for the inner, 120.01% for the center, and 131.04% for the outer modulator bridge designs when the thickness of the bridge was increased from zero to $2\ ^{*}10^{-3}$m. As a result, the iron loss on the modulator ring tends to rise as bridge thickness increases.

Based on bridge arrangements and thicknesses, Fig. 7(d) compares the variability in the peak torque on the low speed rotor. It shows for an increase in thickness from zero to $2^{*}\ 10^{-3}$m, the maximum torque is reduced by 28.02% for the inner bridge, 47.62% for the center bridge, and 79.57% for the outer bridge as the thickness of the bridges is $1^{*}10^{-3}$m.

And also, the peak torque for the inner, center, and outer bridge configuration of modulators on CMG consistently drops by up to 56.9%, 63.3%, and 88.8% with increasing bridge thickness up to $2^{*}10^{-3}$m. As indicated on[63-66], it makes realistic that the thickness of the bridges had better to as thin as possible to maximize the highest possible torque in the CMG, by reducing leakage flux across the modulator carriage bridge.

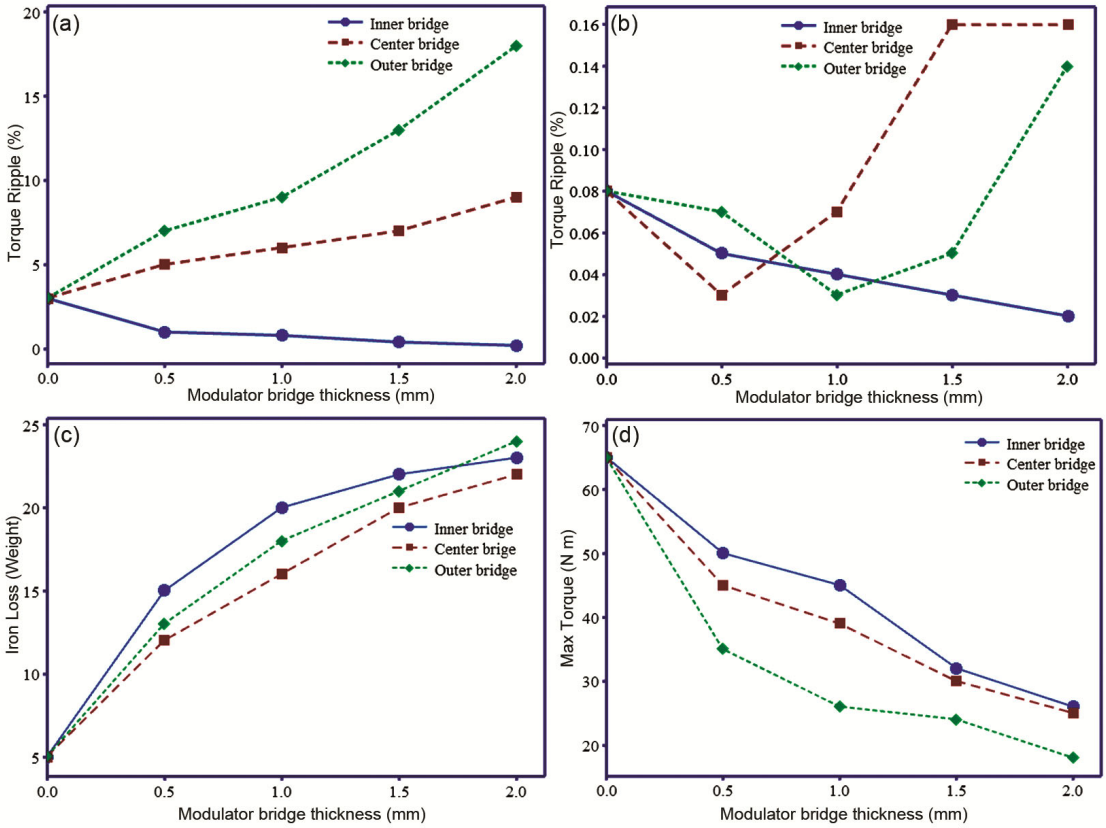

Fig. 7 — Performance evaluation of CMGs based on thickness of the bridge (a) Torque ripple in the inner rotor, (b) Torque ripple in the outer rotor, (c) Iron loss on the modulator, (d) and Maximum output torque, data taken and reproduced[63-66].

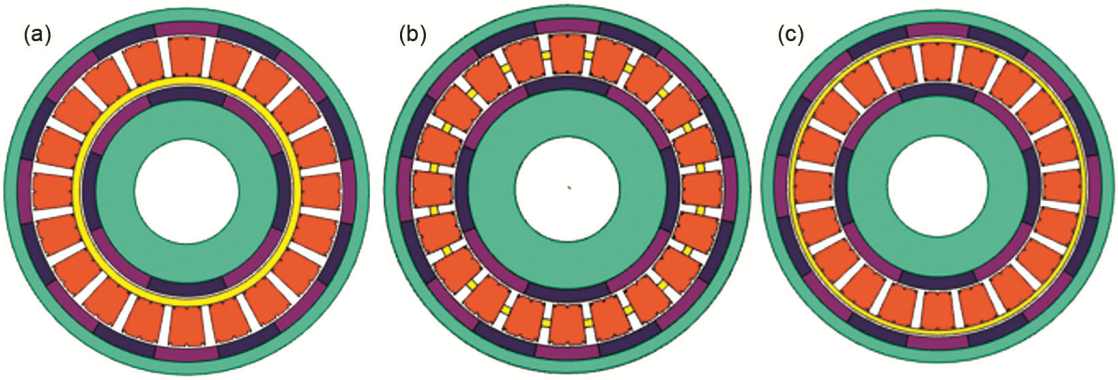

Fig. 8 — Structural illustration of slotted modulator MGs (a) Inner bridge, (b) Center bridge, and (c) Outer bridge.

2.2 Slotted modulator model

All three models have the same gear ratios, volume, and design parameters. The only difference is the configuration of the modulator ring bridge. To study the combined impact of various magnetizations, such as radial, tangential, and Halbach arrays, along with different modulator ring topologies, on CMG performance, as depicted in Figs. 8 (a–c).

The materials used for the inner and outer yokes are iron, and the magnetic modulation ring is composed of silicon steel with good magnetic permeability. In order to ensure comparability, only the modulator holding bridge and magnetizations are varied; all other structural parameters are the same and designed based on Table 2.

Each type of MG has an inner higher speed rotor (HRS) with 4 pole pairs, an outer lower speed rotor (LSR) with 16 pole pairs, and a modulator with 20 segments. The inner and outer air gaps are 1 mm each, and based on Eq. 10, all have the same gear ratio of 4, see Fig. 9.

Table 2 — Design specification of the CMG model

Parameters	Value (mm)	Parameters	Units	Value
Outer diameter of outer stator	70	Outer Poles	Pairs	16
Inner diameter of outer stator	65	Inner Poles	Pairs	4
Outer diameter of pole piece	64	Modulators	Number	20
Inner diameter of pole piece	49	Axial length	mm	60
Outer diameter of inner rotor	20	Inner rotor magnet thickness	mm	5
Airgap thickness inner/outer	1	Stack length of pole pieces	mm	15
One side slotting depth	1	Slotting width	degree	0.4
Thickness of modulator	15	Remanence of PMs	T	1.2

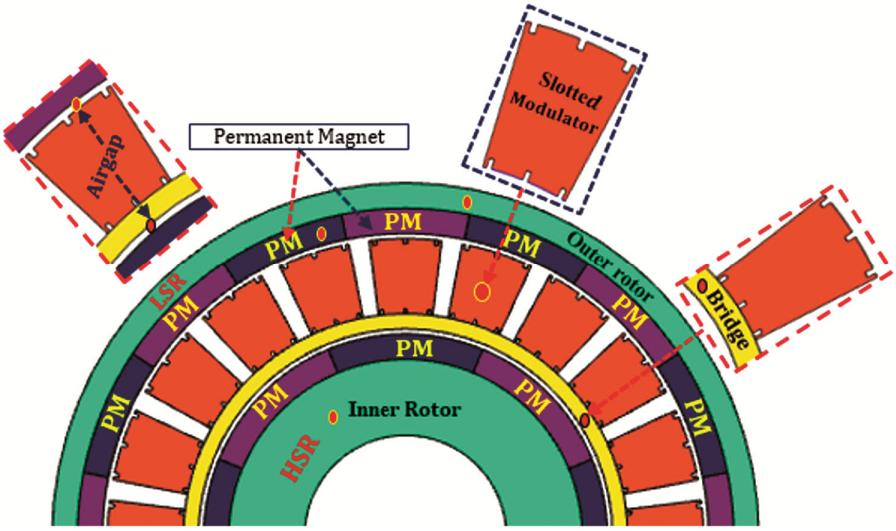

Fig. 9 — Structural description of magnetic gear used for this study.

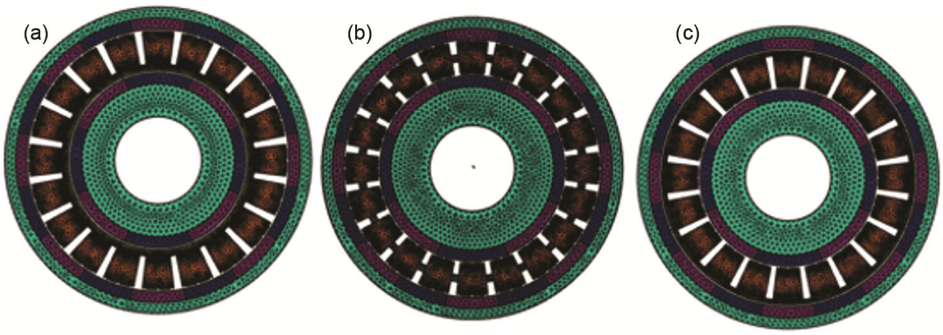

Fig. 10 — Mesh generation for the (a) Inner, (b) Center (c) and Outer modulator bridge configurations of the CMG.

3 Results and Discussion

Based on the findings from previous studies [65–68], the scholars used the finite element method as a computational tool to evaluate the performance of modulator-based magnetic gears (MG). Similarly, this critical review employs the finite element method to computationally evaluate the influence of the modulator connecting bridge design and magnetization on the performance of newly designed modulators in CMG.

The mesh generation for the CMG models is summarized in Table 3. As shown in Figs. 10 (a-c), the type of mesh used throughout the CMG structure is free tetrahedral, with an extra-fine element size to ensure accuracy of the results. The quality of the generated mesh was confirmed by evaluating the skewness range, as depicted in Figs. 11(a–c), for the corresponding bridge configurations.

3.1 Electromagnetic analysis

In a coaxial magnetic gear, the air gap flux density distribution is an important factor influencing the maximum transmitted torque. The inner and outer air gaps are the keys to torque formation.

Table 3 — Mesh details of the designed model

Part name	Element type	Size	Quality (skewness)	Material used
Rotors	Tetrahedral	Extra finer	0.75-0.85	Low carbon steel AISI1008
Permanent Magnets	Tetrahedral	Extra finer	0.75-0.9	NdFeB35
Modulator Ring	Tetrahedral	Extreme finer	0.75-0.85	Low carbon steel AISI1008

Fig. 11 — Mesh quality by using skewness for the above three modulator bridge configurations.

3.1.1 Magnetic torque calculation

One of the crucial characteristics of magnetic gears is their static torque. The torque supplied to the inner and outer rotors, denoted as T_i and T_o, can be determined by utilizing the Maxwell stress tensor following the calculation of the magnetic field distribution in both air gaps [68]. This torque is given as follows:

$$T_i = \frac{Lr^2{}_i}{\mu_0} \int_0^{2\pi} B_p(r_i,\theta)\, B_\theta(r_i,\theta) d\theta \tag{11}$$

$$T_o = \frac{Lr^2{}_o}{\mu_0} \int_0^{2\pi} B_p(r_o,\theta)\, B_\theta(r_o,\theta) d\theta \tag{12}$$

where L is the model's length and r_i and r_o are the two integration pathways' respective radii along the inner and outer air gaps.

The magneto-static force acting on each ferromagnetic pole piece can also be determined by integrating the Maxwell stress tensor along a contour that surrounds it. Consequently, the tangential and radial forces are given as:

$$F_r = \frac{L}{\mu_0} \int_s \frac{B^2 r - B^2 \theta}{2} ds \tag{13}$$

$$F_\theta = \frac{L}{\mu_0} \int_s B_r B_\theta ds \tag{14}$$

The force induced in the tangential direction in the air gap is expressed by the following equations using the Maxwell stress tensor:

$$F = (i_n \frac{B}{\mu_0}) B - i_n \frac{1}{2} \frac{|B|^2}{\mu_0} \tag{15}$$

where B and n denote the normal vectors on the stator surface and the magnetic flux density on the modulator, respectively. Can also be summarized as:

$$F = \frac{1}{\mu_0} (B^2 r - \frac{1}{2} |B|^2) i_r - \frac{1}{\mu_0} B_r B_\theta \, i_\theta \tag{16}$$

The normal direction in Eq. 15 is used to calculate the radial force, and the tangential direction is used to calculate the torques. Therefore, the torque is derived by:

$$T = F_\theta \cdot r = \frac{r}{\mu_0} \int_0^{L_{stk}} B_r B_\theta \, r d\theta dz \tag{17}$$

whereas r denotes the reference point, B_r and B_θ depicts normal and tangential components of the magnetic flux density respectively.

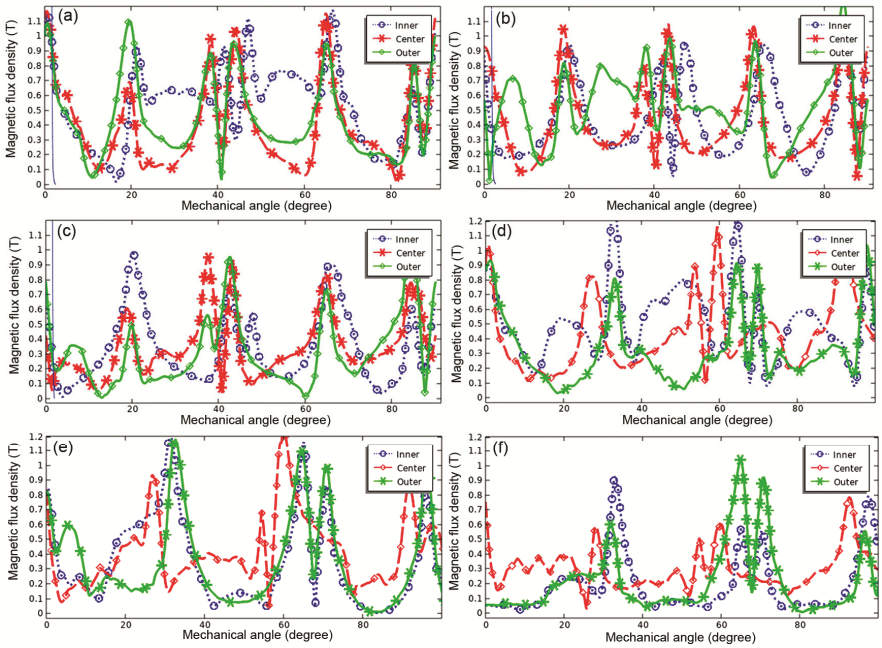

Fig. 12 — Magnetic and flux density plot of rotors (a) Inner radial component, (b) Inner tangential, (c) Inner Halbach (d) Outer radial (e) Outer tangential, and (f) Outer Halbach component.

3.1.2 Magnetic flux density

In order to make the calculation process simpler, the flux density is frequently expressed in the polar coordinate system in 2D design, as shown in Eqs. 5 and 6.

Figure 12 (a–f) depict, the magnetic flux density distribution of the inner and outer rotors of CMGs. By using the mathematical manipulation of the Fourier series, the magnetic flux density results of FEM in the radial, tangential, and Halbach arrangements of the magnetization is depicted in Figs. 12 (a-c) for the inner rotor and Figs. 12 (d-f) for the outer rotor. The magnetic flux density spectrum shows that the modulator having an inner bridge is performing well in all magnetizations for both inner and outer rotor. Fig. 13 depicts the magnetic flux density pattern on a modulating ring for the three distinct modulator ring configurations and magnetizations. The maximum flux density obtained at the modulators for each connecting bridge, as shown in Fig. 13 (a-c), is less than 1.2T. Comparatively discrete Halbach arrays have better magnetic flux density for inner bridge configuration.

Figure 14 (a–f) depict, at the inner and outer air gaps, the magnetic flux density distribution of the slotted modulator of CMGs. By using the mathematical manipulation of the Fourier series, serious decomposition of the magnetic flux density results of FEM in the radial, tangential, and Halbach arrangements of the magnetic field is depicted in Figs. 14 (a-c) for the inner air gap and

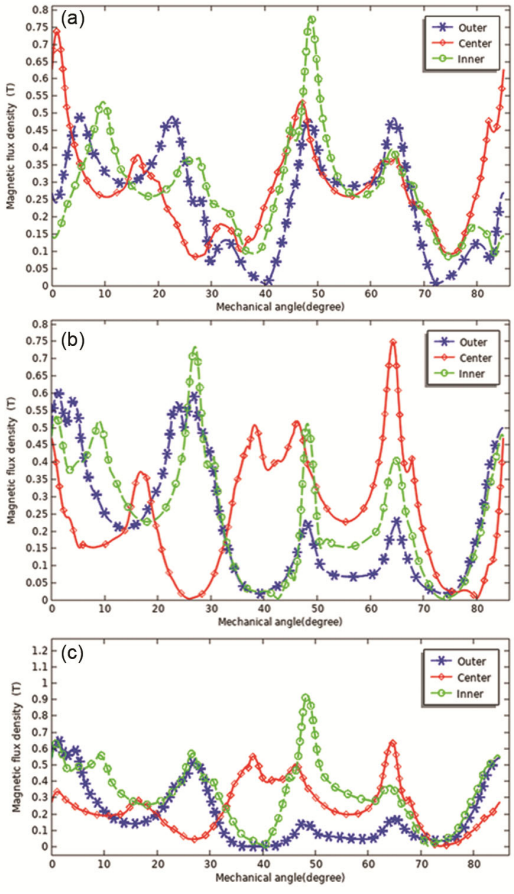

Fig. 13 — Magnetic flux density plot of modulator ring (a) Radial component, (b) Tangential, and (c) Halbach component.

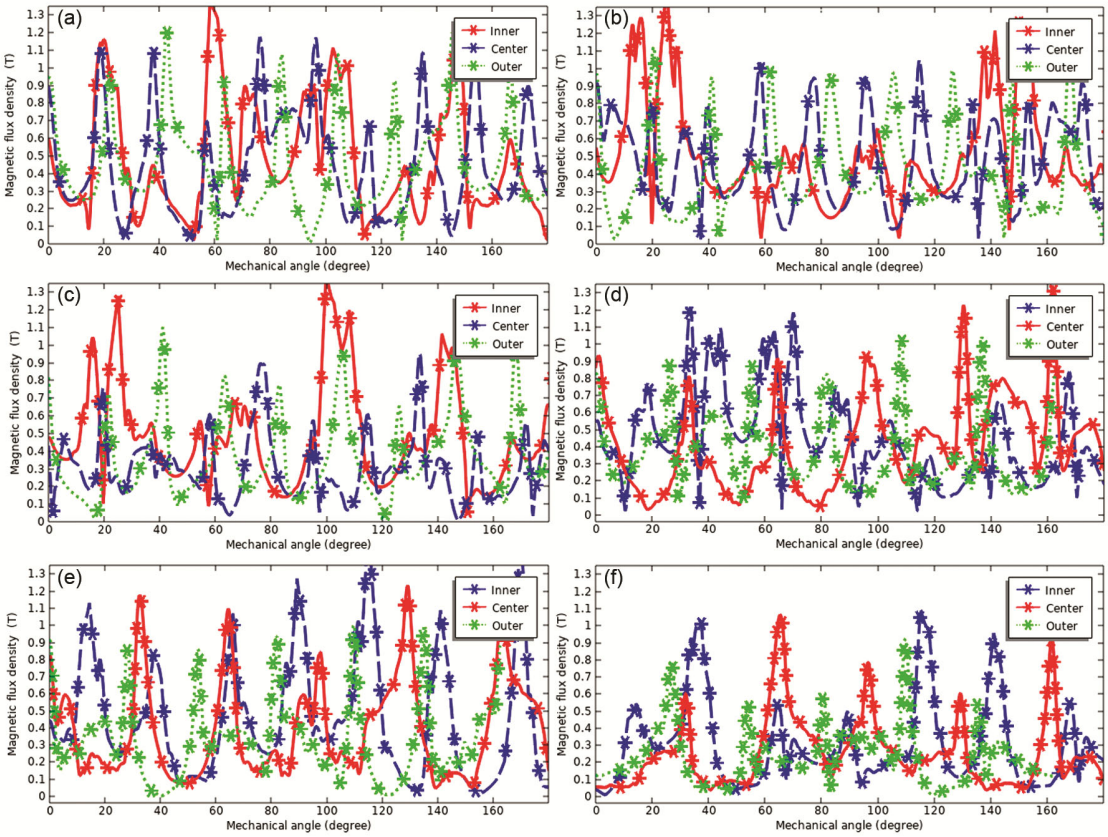

Fig. 14 — Magnetic flux density plot of air gaps (a) Inner radial, (b) Inner tangential, (c) Inner Halbach (d) Outer radial (e) Outer tangential, and (f) Outer Halbach component.

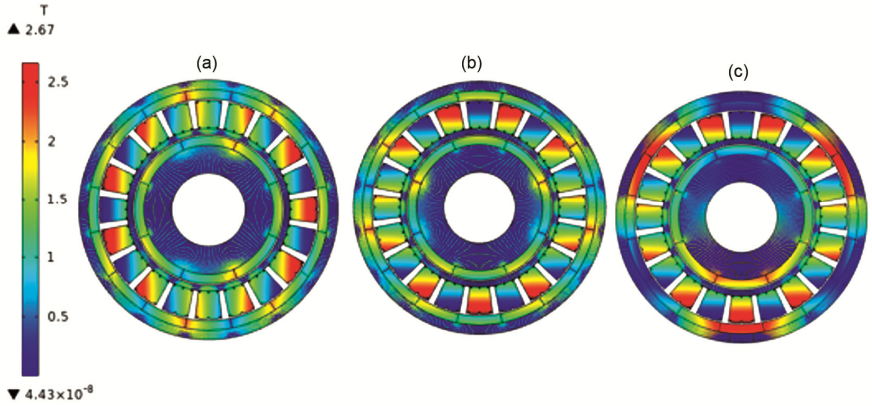

Fig. 15 — Inner bridge slotted modulator magnetic flux density at (a) Radial, (b) Tangential, and (c) Halbach magnetization CMG.

Figs. 14 (d-f) for the outer air gap. The magnetic flux density spectrum shows that the modulator having an inner bridge is performing well in all magnetization's for both inner and outer air gaps; however, it performs best when the magnets have Halbach arrangements (see Figs. 14 (c) & (f) for inner and outer air gaps, respectively); similar findings were reported on different modulator shapes[68].

Therefore, the simulation result shows air gap flux density distribution is an important factor influencing the maximum transmitted torque in coaxial magnetic gear; similar findings were reported on different modulators[67, 68]. However, the bridges tend to interrupt modulation of the air gap flux density owing to considerable flux leakage, which is caused by the closing of the magnetic paths through the bridges.

Figs. 15–17 show the magnetic flux density distribution of the three modeled magnetic modulation ring configurations. Based on Fig. 15

(a-c), when the connection bridge is at the inner location, the maximum flux density by considering three different magnetizations generated at the edge of the modulator is 2.67T when a Halbach array is used. It can be seen from Fig. 16 (a-c) that when the connection bridge is installed at the center, the maximum flux density generated at the modulator is reduced by 4.5% and becomes 2.44T at the Halbach array. It can be seen from Fig. 17 (a-c) that when the connection bridge is installed at the center, the maximum flux density generated at the modulator is reduced by 9.9% and becomes 2.21T; moreover, the Halbach array still has its maximum value. Therefore, regardless of the shape of the modulator, the magnetic flux density tends to be higher at the inner bridge configuration with halbach array magnetization of PMs, which is supported by similar research findings for different modulator shapes [67, 68].

One of the crucial characteristics of magnetic gear is static torque. Fig. 18 (a) depicts how the torque applied to the inner rotor changes while the exterior rotor and modulator ring remain fixed. Theta (θ), which describes the inner rotor's phase angle, ranges from 0 to 90 degrees as it revolutions.

As shown in Figs. 18 (a) and (b), the transmission ratio between the inner and outer rotors of the design MG ratio is 4:1. The static torque waveform of the CMG slotted modulator bridge's three positions is sinusoidal. The CMG with an inner rotor using an outer modulating bridge have the least torque. The Halbach array is used in the analysis owing to its best performance, as shown in Figs. 15–18. The highest electromagnetic torque attained by CMG, with the outer rotor having an inner modular bridge and a Halbach array, is 169 Nm. The remaining CMG torque settings are less than these maximum values, as shown in comparison Fig. 18 (c).

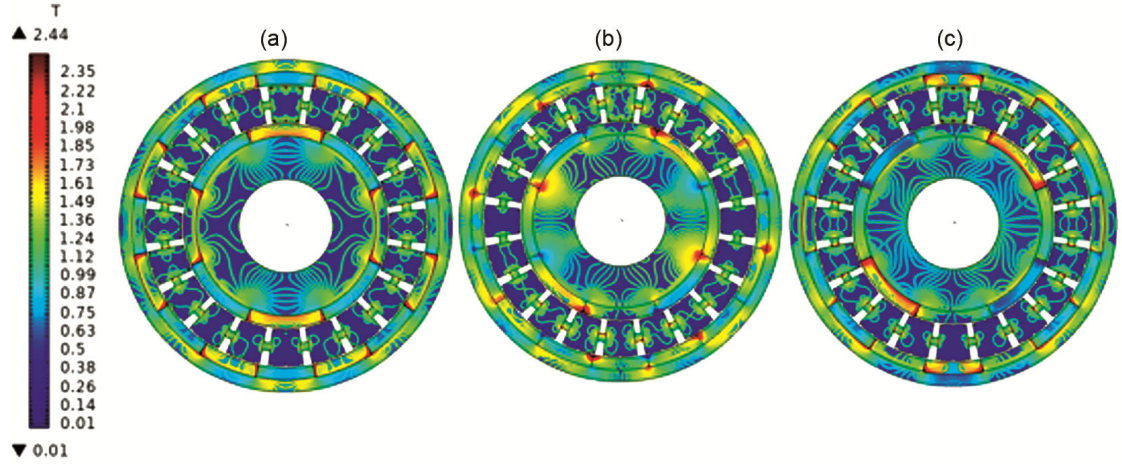

Fig. 16 — Center bridge slotted modulator magnetic flux density at (a) Radial, (b) Tangential, and (c) Halbach magnetization CMG.

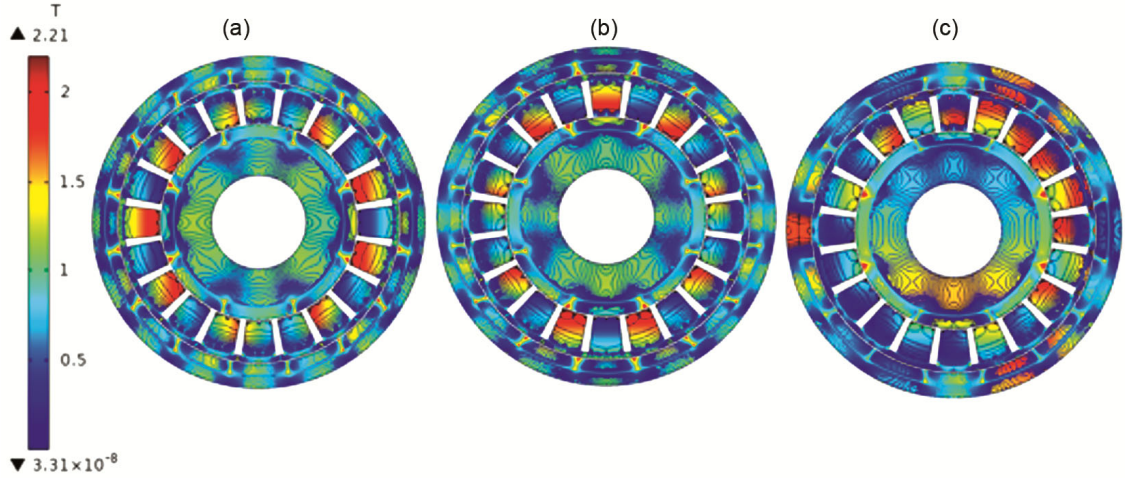

Fig. 17 — Outer bridge slotted modulator magnetic flux density at (a) Radial, (b) Tangential, and (c) Halbach magnetization CMG.

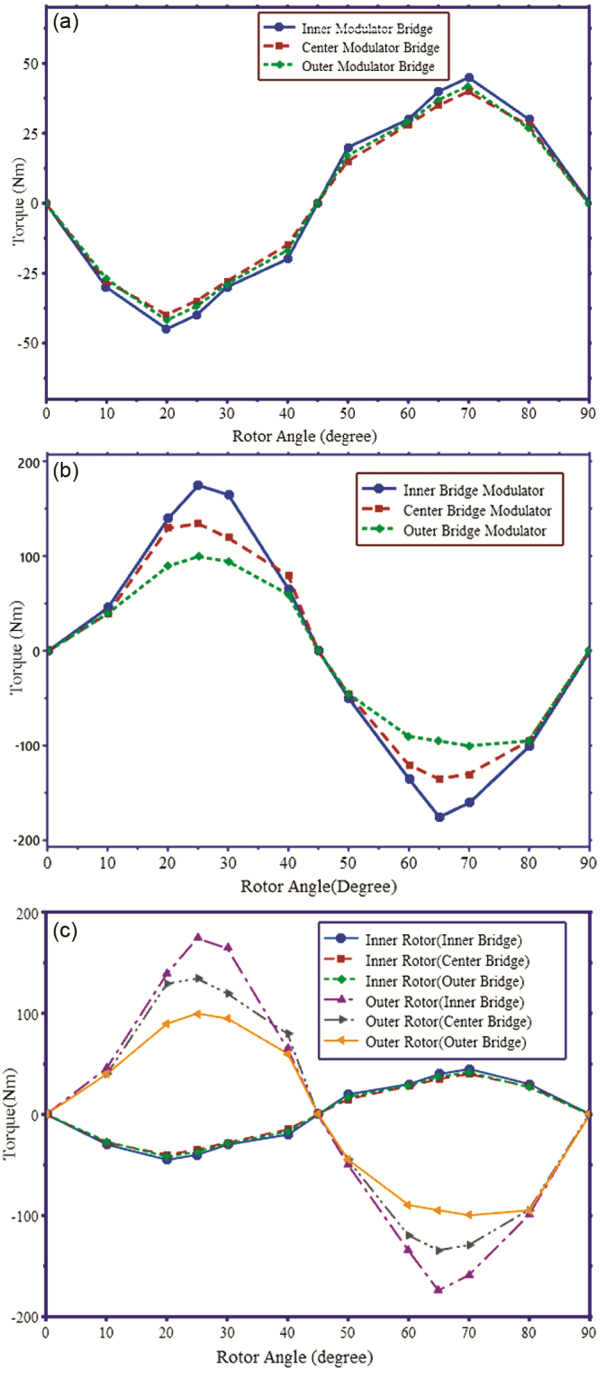

Fig. 18 — Comparison of static torque versus rotor angle curve, (a) Inner rotor, (b) Outer rotor, (c) Both inner and outer rotor.

4 Conclusion

This critical review provides insights into CMG and analyzes the performance of a CMG model with a slotted magnetic modulator. The model incorporates three different linking bridge positions (inner, middle, and outer) and three types of magnetization (radial, tangential, and Halbach array). The comparative analysis was conducted using the 2D nonlinear finite element method, ensuring consistent design parameters and conditions across the studied configurations. The reliability of the study was further validated by comparing the results to similar recent research findings. Based on the review, the key findings are:

- The position and thickness of the bridges are the main parameters influencing the performance of CMGs. The inner modulator bridge type has the best performance in terms of maximum torque and torque ripple; however, it produces large iron losses compared with the other two bridge types. The outer slotted modulator bridge type shows the worst electromagnetic characteristics.
- Furthermore, the middle modulating bridge type performs effectively in terms of reducing iron loss. Hence, CMG applications subjected to higher iron loss at their modulator should use this modulator bridge type rather than the other two.
- Regardless of modulator bridge classification, increasing bridge thickness decreases the entire electromagnetic performance, with the exception of torque ripple. Therefore, in order to increase the performance of CMG, it is desirable to use a modulator bridge that is as thin as possible.
- By keeping all design parameters, such as volume and gear ratios, constant across the three slotted modulator bridge configurations of the CMG, a critical comparison was performed. The results indicate that the CMG with a Halbach array magnetization and an inner modulator bridge position exhibits the highest torque and the lowest torque ripple, compared to the other bridge configurations studied.
- The highest electromagnetic torque attained by CMG when the outer rotor has an inner modular bridge and a Halbach array is 169 Nm.

Acknowledgement

This work was supported by the National Natural Science Foundation of China under Grant 51875254 and State Key Laboratory of Mechanical Transmission for Advanced Equipment Open Fund under Grant SKLMT-MSKFKT-202331.

References

1 Jing B., IEEE Access, 7 (2019) 75550.
2 Leontaritis A., IEEE *Trans. Ind. Appl*, 56 (2020) 4857.
3 Jing B., *IEEE Trans. Ind. Appl*., 56 (2020) 4812

4 Xiang Z., *IEEE Journal of Emerging and Selected Topics in Power Electron*, 10 (2022) 934.
5 Chen Q., *IEEE Trans. Appl. Super Cond*., 3 (2014) 1.
6 Liu H., *IEEE Trans. Magn*., 52 (2016).
7 Park J., *International Conference on Electrical Machines and Systems*, (2017) 11.
8 Fang Z., *IEEE Trans. Energy Con*., 33 (2017) 272.
9 Kjaer R., *IEEE Trans. Energy Con*., 35 (2019) 24
10 Li B., *IEEE Trans. Ind. Appl*, 55 (2019) 55.
11 Klimina S., *Appl. Math. Model*., 46 (2017) 691.
12 Desvaux L., 12th International Conference on Ecological Vehicles and Renewable Energies, (2017) 11.
13 Golovanov G., *International Conference on Electrical Systems for Aircraft*, (2016) 2.
14 Bruzzese L., *International Symposium on Power Electronics*, (2017) 19.
15 Esnoz-Larraya J., *Proceedings of the ESMATS*, (2017).
16 Frandsen V., Proceedings of the *IEEE Energy Conversion Congress and Exposition*, (2012) 3332.
17 Li K., Proceedings of the XIII *International Conference on Electrical Machines (ICEM), IEEE*, (2018) 2016.
18 Wang Y. *et al*., *IEEE Trans. Ind. Appl*., 55 (2019) 4557.
19 Atallah K., *IEEE Trans. Magn.,* 37 (2001) 2844.
20 Jing B., IEEE Access, 8 (2020) 34236.
21 Xiaocun Huang J., *Progress in Electromagnetics Research Letters*, 97 (2021) 69.
22 Chai F., *IEEE Trans. Ind. Electron*, 63 (2016) 3420.
23 Zhang X., *Energies*, 7 (2014) 8535.
24 Neves C., Proceedings of the International Conference on Renewable *Energy Research and Application, IEEE*, (2014), 91.
25 Filippini M., *IEEE Trans. Ind. Electron*, 64 (2017) 9934.
26 Gardner C., *IEEE Trans. Energy Con*., 36 (2021) 2493.
27 Zhu Q., *IEEE Trans. Energy Con*., 15 (2000) 407.
28 Tan C., CES Transactions on *Electrical Machines and Systems*, 7 (2023).
29 Jian C. *et al*., *IEEE/ASME Transactions on Mechatronics*, 24 (2019) 763.
30 Li X., International Conference on Electrical Machines and Systems, (2011) 1.
31 Wang M., Progress in *Electromagnetics Research Magnetics*, 97 (2020) 215.
32 Kim K., *IEEE T. Magn*, 53 (2017) 1.
33 Abdelhamid K., IEEE T. Magn., 53 (2017) 1.
34 Dianati A., *IEEE Trans. Magn*., 52 (2016) 1.
35 Jing B. *et al*., *IEEE T. Appl. Supercon*., 29 (2019) 1.
36 Praslicka, M.J., *IEEE Journal of Emerging and Selected Topics in Power Electronics*, (2021) 3053544.
37 Shin H., *AIP Adv*., 7 (2017) 4973798.
38 Lubin T., *IEEE Trans. Magn*, 46 (2010) 2611.
39 Jian S., *Appl. Math. Model.* 39 (2015) 5746.
40 Zhang X., *et al*., *Energies,* 7 (2014) 8535.
41 Misron N., *Appl. Sci*., 10 (2020) 1.
42 Yin X., *IEEE Int. Magn. Conf*., (2015) 4095.
43 Tang Z., *IEEE Trans. Magn*., 9464 (2021) 8.
44 Pollok S., *IEEE Trans. Magn*., (2021) 3082431.
45 Wang J., *IEEE Trans. Magn*., 47 (2011) 4477.
46 Huang C. *et al*., *IEEE Trans. Magn*., 44 (2008) 403.
47 Jorgensen T., *IEEE Trans. Ind. Appl*., 44 (2008) 1659.
48 Pakdelian S., *IEEE Energy Convers. Congr. Expo*. (2012) 3340.
49 Rens, D.H., *IEEE Trans. Ind. Appl.*, 46 (2010) 206.
50 Atallah K., H., *IEEE Proceedings Electric Power Applications*, 151 (2004) 135.
51 Filippini A., *IEEE T. Ind. Electron*, 64 (2017) 9934.
52 Tuma J., *Wiley Hoboken, NJ, USA*, 9781118359419 (2014).
53 Chau, M. Cheng, and W. Hua, *Prog. Electro. Magn. Res*., 133 (2013) 177.
54 Chiang D. and S. Wang, *IEEE Trans. Magn*., 33 (1997) 2203.
55 Cho H. and H. Shin, Proceedings of the 2015 *IEEE Magn. Conference*, 9 (2015) 1059.
56 Asnani T., Magnetic gearing research at NASA, Proc. of AHS Intl. 74th Annual Forum Phoenix, (2018).
57 Gerber W., *IEEE T. Magn*., 51 (2015) 1.
58 Wang J., *et al*., *IEEE Magn. Letters*, 7 (2016) 1.
59 Li W., *IET Electr. Power App*., 12 (2018) 231.
60 Liu Q., *IEEE Trans. Magn*., 57 (2021) 1.
61 Ren X., *IEEE Trans. Ind. Electron*., 67 (2020) 6248.
62 Kim P., *21st International Conference on Electrical Machines and Systems*, JEJU, Korea, (2018) 2497.
63 Gardner C., *IEEE Trans. Ind. Appl*., 54 (2018) 2237.
64 Johnson M., IEEE *Trans. Ind. Appl*., 54 (2018) 1254.
65 Aiso K., 2020 *IEEE Energy Conversion Congress and Exposition*, (2020) 68.
66 Ni X., *IEEE Trans. Magn*., 56 (2020) 1.
67 Pakdelian S., *IEEE Trans. Ind. Electron*, 67 (2020) 9582.
68 Zhang C., A *IEEE T. Energy Conver*, 33 (2018) 682.